

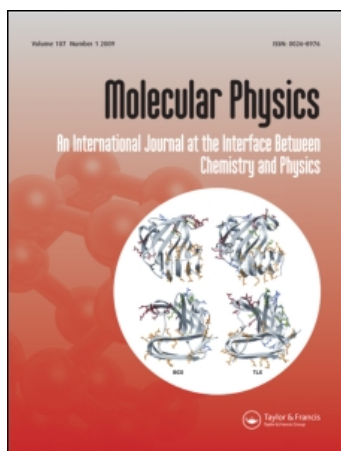
This article was downloaded by: [University of Oxford]

On: 9 March 2010

Access details: Access Details: [subscription number 909667648]

Publisher Taylor & Francis

Informa Ltd Registered in England and Wales Registered Number: 1072954 Registered office: Mortimer House, 37-41 Mortimer Street, London W1T 3JH, UK



## Molecular Physics

Publication details, including instructions for authors and subscription information:

<http://www.informaworld.com/smpp/title~content=t713395160>

### Cavity enhanced detection methods for probing the dynamics of spin correlated radical pairs in solution

Simon R. T. Neil <sup>a</sup>; Kiminori Maeda <sup>bc</sup>; Kevin B. Henbest <sup>ab</sup>; Martin Goez <sup>bd</sup>; Robert Hemmens <sup>b</sup>; Christiane R. Timmel <sup>bc</sup>; Stuart R. Mackenzie <sup>a</sup>

<sup>a</sup> Department of Chemistry, University of Oxford, Physical and Theoretical Chemistry Laboratory, Oxford OX1 3QZ, UK <sup>b</sup> Department of Chemistry, University of Oxford, Inorganic Chemistry Laboratory, Oxford, OX1 3QR, UK <sup>c</sup> Centre for Advanced Electron Spin Resonance, Oxford, OX1 3QR, UK <sup>d</sup> Institut für Chemie, Martin-Luther-Universität Halle-Wittenberg, Germany

First published on: 09 March 2010

**To cite this Article** Neil, Simon R. T., Maeda, Kiminori, Henbest, Kevin B., Goez, Martin, Hemmens, Robert, Timmel, Christiane R. and Mackenzie, Stuart R.(2010) 'Cavity enhanced detection methods for probing the dynamics of spin correlated radical pairs in solution', Molecular Physics,, First published on: 09 March 2010 (iFirst)

**To link to this Article:** DOI: 10.1080/00268971003614368

**URL:** <http://dx.doi.org/10.1080/00268971003614368>

## PLEASE SCROLL DOWN FOR ARTICLE

Full terms and conditions of use: <http://www.informaworld.com/terms-and-conditions-of-access.pdf>

This article may be used for research, teaching and private study purposes. Any substantial or systematic reproduction, re-distribution, re-selling, loan or sub-licensing, systematic supply or distribution in any form to anyone is expressly forbidden.

The publisher does not give any warranty express or implied or make any representation that the contents will be complete or accurate or up to date. The accuracy of any instructions, formulae and drug doses should be independently verified with primary sources. The publisher shall not be liable for any loss, actions, claims, proceedings, demand or costs or damages whatsoever or howsoever caused arising directly or indirectly in connection with or arising out of the use of this material.

## Cavity enhanced detection methods for probing the dynamics of spin correlated radical pairs in solution

Simon R.T. Neil<sup>a</sup>, Kiminori Maeda<sup>bc</sup>, Kevin B. Henbest<sup>ab</sup>, Martin Goetz<sup>bd</sup>,  
Robert Hemmens<sup>b</sup>, Christiane R. Timmel<sup>bc\*</sup> and Stuart R. Mackenzie<sup>a\*</sup>

<sup>a</sup>Department of Chemistry, University of Oxford, Physical and Theoretical Chemistry Laboratory,  
South Parks Road, Oxford OX1 3QZ, UK; <sup>b</sup>Department of Chemistry, University of Oxford,  
Inorganic Chemistry Laboratory, South Parks Road, Oxford, OX1 3QR, UK; <sup>c</sup>Centre for Advanced Electron  
Spin Resonance, South Parks Road, Oxford, OX1 3QR, UK; <sup>d</sup>Institut für Chemie,  
Martin-Luther-Universität Halle-Wittenberg, Kurt-Mothes-Str. 2, D-06120 Halle, Germany

(Received 20 October 2009; final version received 11 January 2010)

Cavity enhanced absorption spectroscopy (CEAS) combined with phase-sensitive detection is employed to study the effects of static magnetic fields on radical recombination reactions. The chemical system comprises the photochemically generated thionine semiquinone radical and a 1,4-diazabicyclo[2.2.2]octane (DABCO) cationic radical in a micellar solution of sodium dodecyl sulphate. Data obtained using the modulated CEAS technique, describing the magnetic field effect (MFE) on reaction yields, are shown to be superior to those obtained using conventional transient absorption (TA) flash photolysis methods typically employed for these measurements. The high sensitivity afforded by modulated CEAS detection is discussed in terms of the new possibilities it offers such as the measurement of magnetic field effects in real biological systems which have hitherto been largely beyond the detection capabilities of existing techniques.

**Keywords:** Cavity ring-down; cavity enhanced absorption; spin chemistry; radical pair mechanism; magnetic field effects

### 1. Introduction

With the notable exception of the short-lived radical pair intermediates involved in the initial steps of photosynthesis [1–3], little attention has been focused on the investigation of magnetosensitive reactions in biologically relevant systems *in vitro* [4]. However, the recent discovery in organisms ranging from plants to insects, birds and humans [5,6], of cryptochrome, a 55 kDa, blue light receptor protein, and the suggestion of its key role in the processes controlling the avian magnetocompass [7] have resulted in the observation of a magnetic field dependent radical reaction in the cryptochrome-related photolyase protein [8]. These findings have sparked extensive searches for further magnetosensitive biological systems.

By contrast, the effects of both static and oscillating magnetic fields have been studied in a plethora of chemical systems involving radical pair (RP) intermediates [9–12]. Measurements of the magnetic field effects (MFE) on either the yield or the kinetics of the radical recombination reactions are, with the exception of photoconductivity or HPLC measurements, nearly exclusively based on optical detection methods.

Investigation of RPs recombining *via* a fluorescing exciplex allows the direct detection of the reaction yield by a zero-background technique whilst facilitating the employment of modulation techniques and lock-in detection rendering these experiments exceptionally sensitive. Despite the deep physical insight yielded by this technique, however, magnetosensitive measurements of radical reactions have, on the whole, been limited to a handful of emissive chemical systems [9,10].

The vast majority of RP reactions have been studied using absorption techniques. These methods frequently suffer from low sensitivity as the absorption signal is usually observed as a small decrease in light intensity measured on a large background. Typically, flash photolysis experiments are employed which facilitate time-resolved studies, but exclude the employment of modulation techniques combined with lock-in detection to improve the sensitivity of measurements. In order to compensate for the limited detection sensitivity, most studies to date have used high concentrations and long averaging times. To mitigate against the effects of photodegradation, large sample volumes are also typically required. The biological samples of most interest,

\*Corresponding authors. Email: christiane.timmel@chem.ox.ac.uk; stuart.mackenzie@chem.ox.ac.uk

however, such as photolyases and cryptochromes mentioned above, cannot be produced in the (millilitre) volumes and (millimolar) concentrations needed to obtain high quality data. Concentrating these protein solutions frequently leads to precipitation and clouding of the solution. Furthermore, any *in vitro* studies at concentrations reflecting typical *in vivo* conditions are simply not feasible. There is, therefore, an acute need for high-sensitivity detection methods to facilitate meaningful magnetic field effect studies of biologically relevant systems.

Optical cavity-based absorption techniques, in particular the numerous variants of cavity ring-down spectroscopy (CRDS) [13–15] and cavity enhanced absorption spectroscopy (CEAS) [16,17], are well-established methods for the detection of highly dilute or weakly absorbing gas-phase species. Both methods take advantage of the enormously increased optical path lengths which may be achieved from multiple passes through a sample located within a high-finesse cavity. In CRDS, a pulse of light (typically from a laser source) is injected into the optical cavity and the rate of decay of the light circulating, characterised by the ring-down time,  $\tau$ , is measured.  $\tau$  provides a direct measure of the total round-trip losses which, in turn, can yield absorbance or scattering losses arising from an intracavity sample [14]. In CEAS, similar information is extracted from the intensity of the light transmitted through the cavity during continuous optical pumping.

Despite their versatility and the simplicity of their implementation, optical cavity based techniques have been used much less for investigating condensed phase systems than for the gas phase. They are, however, becoming increasingly popular [18,19]. Early applications of liquid-phase CRDS included the use of intra-cavity liquid cells placed at Brewster's angle to the cavity (optical) axis [20] or simply filling the cavity with liquid sample [21,22]. More recently, various elegant approaches have been developed such as the use of liquid jets aligned at Brewster's angle [23] and evanescent wave variants for the study of interfacial phenomena including surface kinetics [24–26]. However, the use of cuvettes remains the most common variant, both for the study of solution kinetics and, using precision optical cells, as an alternative to UV-visible spectroscopy in HPLC detection [20,27–30].

Condensed phase applications of CEAS are even more scarce than those of CRDS despite the fact that larger dynamic ranges may be achieved [31,32]. In this article we describe a combination of fixed wavelength CRDS and frequency modulated CEAS, applied to the measurement of magnetic field effects on reaction yields.

### 1.1. The radical pair mechanism

All chemical reactions known to be affected by magnetic fields proceed *via* a mechanism involving pairs of spin-correlated radicals [9]. These radical pairs (RPs) are typically produced *via* photolytic bond cleavage under conservation of total electron spin angular momentum so that a singlet (triplet) molecular precursor leads to a singlet (triplet) arrangement of the spins in the two geminate radicals. The RP subsequently undergoes coherent spin evolution between the singlet (S) and triplet (T) states, a process which can be influenced by applied static and/or oscillating magnetic fields. At zero field and in the absence of exchange and dipolar interactions, the S- and three T-levels are degenerate and interconversion is driven efficiently by the interaction between the electron spins and surrounding magnetic nuclei. The application of a weak magnetic field (i.e. a field smaller than the average hyperfine coupling in the RP) can, however, activate coherences dormant at zero-field, accelerating ST mixing [33–35]. Conversely, magnetic fields exceeding the average hyperfine coupling, help separate the  $S/T_0$  sub-levels from the  $T_{+1/-1}$  manifold thereby hampering efficient ST interconversion. As a result radicals may become trapped in the  $T_{+1/-1}$  states from which no recombination is allowed [36]. These two effects are referred to as Low Field Effect (LFE) and 'normal' MFE, respectively, see Figure 1.

The yield of the radical reaction is sensitive to magnetic fields only if the recombination of singlet and triplet RPs yields different products. Typically, it is only the singlet RPs that, upon reencounter, can recombine to produce the original molecular precursors. Therefore, an acceleration of ST mixing in a triplet-born RP leads to an increase in the (singlet-formed) recombination product and a concomitant reduction in the number of triplet-formed free radicals escaping the solvent cage. If recombination through singlet and triplet channels occurs at different rates, the overall reaction kinetics will be magnetic field dependent [37,38]. However, the hyperfine-induced ST mixing takes a finite time (for carbon-centred radicals, typically  $\sim 10$  ns). Furthermore, the MFE might be quenched by rapid spin relaxation, radical recombination and/or escape. As a result, for the static fields used here, 0–20 mT, in order to observe a MFE, the spin correlation and RP lifetimes should exceed 10 ns.

The recombination of triplet born RPs, to triplet excited states, is rare. Escape processes are, therefore, crucial in determining the lifetime of the radical pair. For this reason, microreactors such as micelles are often employed in MFE experiments to prolong the lifetime of the geminate radical pair.

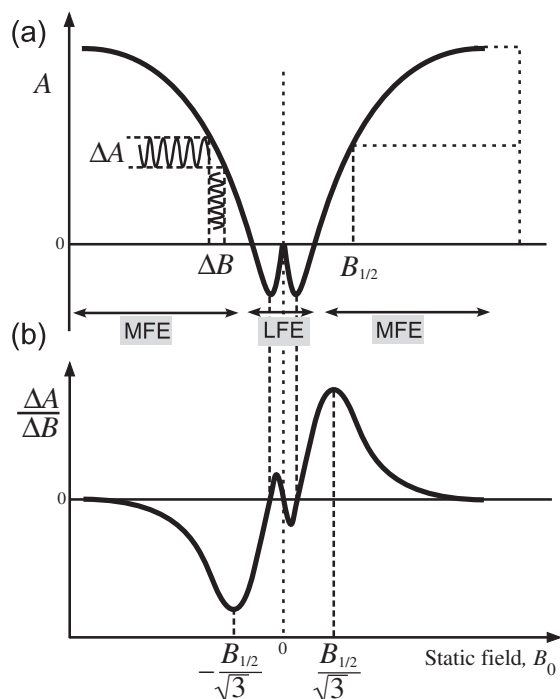


Figure 1. (a) A typical magnetic field effect spectrum shown for a triplet born RP. The signal,  $A$ , might correspond to the absorbance of one of the radicals. The decrease in  $A$  in the low field region and the increase at higher field are explained by the LFE and ‘normal’ MFE mechanisms, respectively.  $B_{1/2}$  is defined as the field at half of the saturation value of the MFE. The field is modulated, typically at audio frequencies, and with modulation depth,  $\Delta B$ , leading to a modulation in the resulting signal,  $\Delta A$  (b) Phase sensitive detection records the first derivative ( $\Delta A/\Delta B$ ) of the expected MFE graph. For a Lorentzian function, peaks in the first derivative spectrum occur at  $\pm B_{1/2}/\sqrt{3}$ .

## 2. Experimental

### 2.1. The photochemical system

The chemical system chosen for this study comprises the photochemical dye thionine ( $\text{TH}^+$ ) and 1,4-diazabicyclo[2.2.2]octane (DABCO) (Figure 2(a)) in a micellar solution of sodium dodecyl sulphate (SDS). Green light irradiation of the solution produces the excited singlet state of thionine,  $^1\text{TH}^{+*}$  (see Figure 2(b)) for the absorption profile of  $\text{TH}^+$  featuring a strong band at 600 nm with a weak tail at 532 nm). Figure 2(c) shows the photochemical reaction scheme. Following production of the  $^1\text{TH}^{+*}$  excited state, intersystem crossing to the  $^3\text{TH}^{+*}$  state occurs on a picosecond timescale [39]. Quenching of  $^3\text{TH}^{+*}$  with DABCO produces the spin-correlated radical pair,  $^3[\text{TH}^\bullet + \text{DABCO}^{+\bullet}]$ , under conservation of total spin angular momentum. The efficiency of the subsequent  $^3[\text{TH}^\bullet + \text{DABCO}^{+\bullet}] \leftrightarrow ^1[\text{TH}^\bullet + \text{DABCO}^{+\bullet}]$  interconversion (and, hence, the radical yield of the

photochemical reaction) is magnetic field dependent as discussed above.

The intense absorption band of the  $\text{TH}^\bullet$  radical, centred around 400 nm, allows selective detection of this species using a 405 nm diode laser without spectral overlap with the  $\text{TH}^+$  species, see Figure 2(b). Once radical species escape from the geminate solvent cage, they can only decay by bulk encounter and thus exhibit very long lifetimes ( $\sim \mu\text{s}$  to ms). Encounters between separated radicals are always unreactive if the RP is in a triplet state but singlet state encounters may lead to recombination.

The RP molecular precursors are dissolved in a micellar solution of SDS to prolong the lifetime of the geminate radical pair thereby maximising the observed magnetic field effect. The exact location of the molecules/radicals with respect to the micelle (core/Stern layer/bulk) is not entirely certain. Previous work on the related DABCO/Xanthone(Xa) system indicates that, at the moment of creation from its molecular precursor,  $\text{DABCO}^{+\bullet}$  is located just outside the micelle, on the opposite side of the phase boundary to the hydrophobic Xa which inhabits the micelle interior [40]. The surface charge of the micelle leads to  $\text{DABCO}^{+\bullet}$  being trapped within the negatively-charged Stern layer of the SDS micelle whilst  $\text{Xa}^{-\bullet}$  escapes the negatively charged micro-reactor only slowly. For the DABCO/ $\text{TH}^+$  system used here, the situation at the moment of the birth of the radical pair is likely to be very similar because the positively charged ground-state sensitiser  $\text{TH}^+$  will initially be located on the negatively charged micelle surface. The uncharged and slightly hydrophobic sensitiser-derived radical enters the micelle, whilst the DABCO radical cation is trapped in the Stern layer. It is thus likely that both radicals are found in or near the Stern layer leading to a much prolonged lifetime of the geminate RP compared with that in homogeneous solution and hence a significant MFE.

### 2.2. Materials

Solutions were made up in ultrapure Milli-Q water. A small aliquot of a stock solution of thionine (Aldrich) in water was added to a solution of 10 mM SDS, followed by addition of aqueous DABCO (0.2 M). The thionine concentrations used for individual experiments are specified later. During experiments, all solutions were continually purged with nitrogen to eliminate dissolved oxygen, thereby minimising the quenching of the thionine triplet state in solution. The pH of the solution was approximately 11.

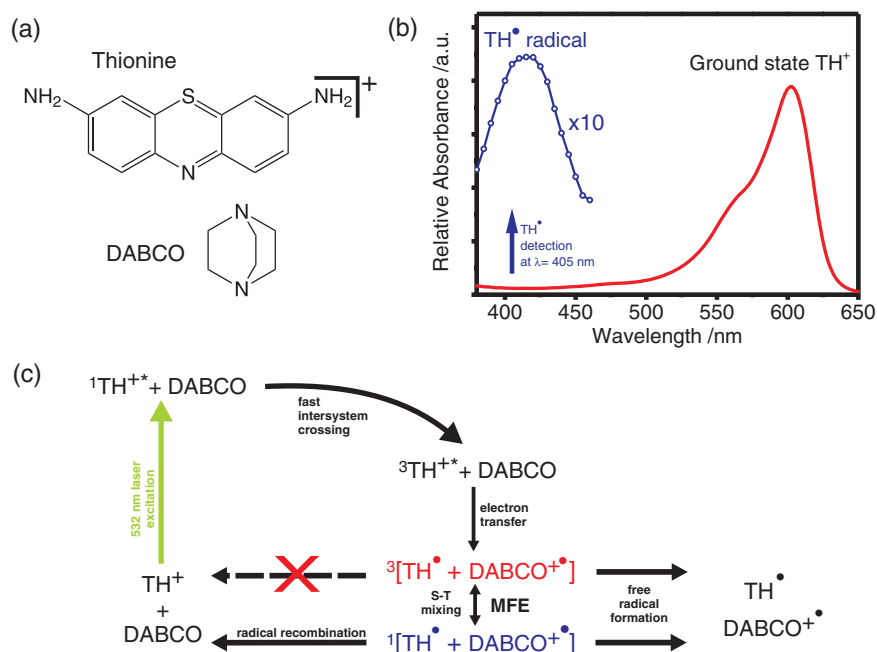


Figure 2. [colour online] (a) Structures of the RP molecular precursors, thionine and DABCO. (b) Relative absorption spectra for the thionine ground state and the neutral TH<sup>•</sup> radical. (c) Photochemical reaction scheme for the TH, DABCO system in a micellar solution of SDS.

### 2.3. CRDS and frequency modulated CEAS

The experimental apparatus and optical arrangement are shown schematically in Figure 3, and comprise four main components: (i) an optical cavity, (ii) an excitation source for radical generation (iii) a 405 nm diode probe laser and photomultiplier tube (PMT) for radical detection, and (iv) a Helmholtz coil arrangement for applying modulated magnetic fields. The centre piece of the experiment is the intra-cavity thin layer cuvette (in this study a fused-silica EPR cell) through which the solution is continually flowed such that the cavity axis, magnetic field and the flow direction are mutually perpendicular.

The high-finesse optical cavity is formed using two highly reflective concave mirrors (Los Gatos Research, Reflectivity = 0.99995 at 405 nm, radius of curvature 1 m) mounted 12 cm apart on individual precision gimbal mounts. The sample cell (Starna Scientific, UV Quartz, 1 mm path length) is carefully oriented normal to the optical cavity by mounting it on a rotation stage. This geometry ensures that any reflections from the surfaces of the cell are not lost from the cavity. Attempts were initially made to mount the cell at Brewster's angle to the cavity axis in order to minimise these reflective losses, but for these experiments such an arrangement proved less satisfactory than the normal configuration.

Light from a CW diode laser (Laser Quantum, Torus, 532 nm), is used to generate the electronically excited <sup>1</sup>TH<sup>+\*</sup> radicals. Various laser powers, specified for individual experiments, are used. A four-pass bow-tie arrangement of the photoexcitation laser through the sample (see Figure 3) increases the concentration of radicals generated and thus the signal to noise ratio (SNR) achieved. Optical alignment of the 532 nm laser path is ensured by maximising the CRDS-monitored absorbance within the sample cell (see below).

The detection light source is a 405 nm diode laser (Power Technology, 1Q1H, 405 nm, maximum power output 400 mW, line width *ca* 1 nm) and the light transmitted through the cavity is detected using a PMT (either Electron Tubes, Q-9893 or Hamamatsu R928). Switching between CRDS and modulated CEAS experiments can be done without modifying the optical arrangement. For CRDS measurements, the detection laser is pulsed at a frequency of 3 kHz using an external pulse generator (TTi, TGP 110). Every time the laser is switched off, the light intensity within the cavity decays exponentially with a 'ring-down' time,  $\tau$ , characteristic of the losses per round trip. As well as surface and bulk scattering losses, these include the absorbance within the sample itself. Ring-down traces are recorded on a 12 bit 200 MS/s PC acquisition card

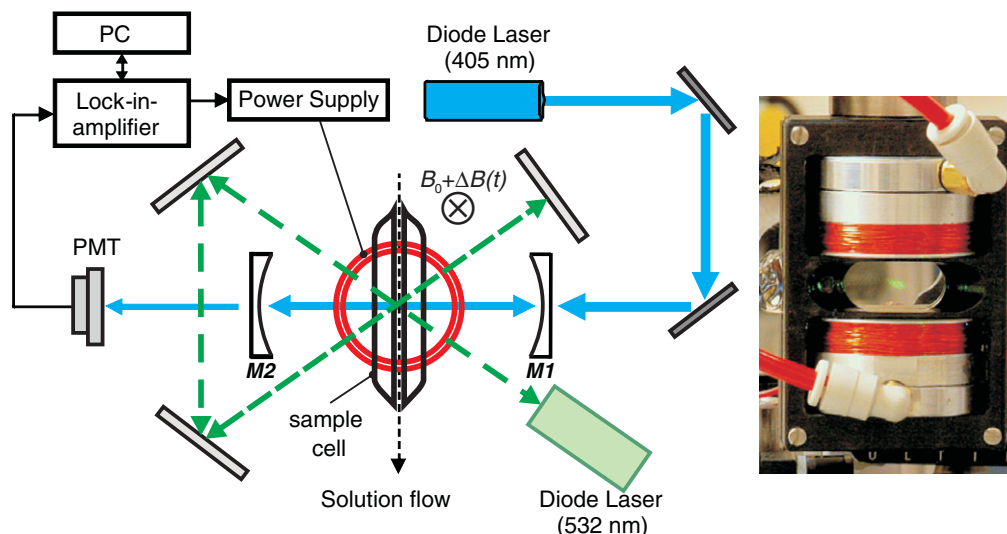


Figure 3. [colour online] Schematic of the experimental arrangement for modulated CEAS. A pair of Helmholtz coils (indicated by concentric circles) used to generate the magnetic field,  $B = B_0 + \Delta B(t)$ , surround the sample cell which lies at the centre of an optical cavity formed by mirrors M1 and M2. The 532 nm photo-excitation beam (dashed arrows, in green online) is arranged in a 4-pass bow-tie arrangement. Inset: The mounted sample cell, with Helmholtz coils above and below, as viewed along the optical axis of the high finesse cavity. The 532 nm laser beam spot is visible in the centre of the cell.

(National Instruments PCI-5124) from which  $\tau$  is extracted *via* a Fast Fourier transform method using LabVIEW©.

Before every modulated CEAS experiment, CRDS is used to determine the absolute absorbance of  $\text{TH}^\bullet$  within the intra-cavity cell at  $B=0$ . The cavity and sample cell are aligned to maximise the ring-down time with Milli-Q water flowing through the cell. The DABCO, thionine and SDS solution is then flowed through the cell using a gravity-fed arrangement between two reservoirs. An alternative, peristaltic pump system was found to introduce additional noise. A flow rate of 3 mL/min, chosen to maximise the CRDS SNR, is maintained by means of a tap placed in the flow path after the sample cell and the solution is recycled between the reservoirs. Continual sample flow is essential to mitigate against the effects of photodegradation. The cavity ring-down time, recorded in the absence,  $\tau_0$ , and presence,  $\tau_1$ , of the 532 nm photo-excitation light, is used to calculate the  $\text{TH}^\bullet$  absorbance per pass,  $A$  (in conventional  $\log_{10}$  scale) using:

$$2.3026A = \frac{\tau_0 - \tau_1}{\tau_1 \tau_0} \left( \frac{L}{c} \right), \quad (1)$$

in which  $L$  is the length of the cavity and  $c$  the speed of light. The corresponding  $\text{TH}^\bullet$  concentration ( $[\text{TH}^\bullet]_{B=0}$ ) is calculated *via* the Beer–Lambert law, using the known radical extinction coefficient ( $11426 \text{ M}^{-1}\text{cm}^{-1}$ , in methanol) at 405 nm [39]. This direct link in CRDS between the measured ring-down time and

the absolute absorbance is invoked in this study to determine  $\text{TH}^\bullet$  radical concentrations.

Since  $\tau_0$  reflects all cavity losses except the  $\text{TH}^\bullet$  absorption, it is strongly dependent on (i) the alignment of the entire cavity, (ii) the cleanliness of the cell and (iii) any additional losses (scattering and absorbance) within the aqueous DABCO, SDS and thionine solution not due to radical absorption.  $\tau_0$  is typically 150–185 ns which represents 375–460 sample passes before the light intensity in the cavity drops by a factor  $1/e$ . For comparison, the ring-down time obtained with pure water in the cell is typically 300–400 ns (750–1000 passes). The additional losses arising from the sample, are probably dominated by scattering of the micelles with minor absorption losses due to reactant precursors.

Following CRDS measurements, and without change to the cavity alignment, modulated CEAS is performed. In CEAS, light is continuously pumped into the cavity. Under these conditions, the light intensity within the cavity rapidly reaches a steady state directly proportional to the ring-down time. Unlike CRDS, CEAS does not provide an absolute absorbance directly. To determine absorbances, it is necessary to compare the transmitted light intensity,  $I$ , with that,  $I_0$ , recorded in the absence of the absorber. The absolute absorbance,  $A$ , is then given by

$$2.3026A = \left( \frac{I_0}{I} - 1 \right) (1 - R_{\text{eff}}). \quad (2)$$

In this implementation,  $R_{\text{eff}}$  represents an effective reflectivity, incorporating not only the reflectivity of the cavity mirrors (as in the case of gas-phase absorptions), but also light losses due to the intracavity sample cell and scattering losses in the sample. The effect of the optical cavity is to increase the effective path length, compared to a traditional single-pass experiment, by a factor of  $(1 - R_{\text{eff}})^{-1}$ , sometimes referred to as the cavity enhancement factor (CEF). For the modulated CEAS measurements, the pulse generator is turned off and the 405 nm diode laser operates in continuous wave mode. Light exiting the cavity is directed, using a liquid light guide, onto a PMT, the output of which is connected to signal and auxiliary inputs on a lock-in amplifier (LIA, Stanford research systems SRS510) to permit phase-sensitive detection and direct monitoring of the PMT output, respectively.

To enable the recording of modulated CEAS MFE spectra, the sample cell is mounted between a pair of water-cooled Helmholtz coils (see Figure 3), which provides swept and modulated homogeneous magnetic fields in the sample region. The applied field is varied from  $-15$  to  $+15$  mT, through zero. In addition, the magnetic field is audiofrequency-modulated, at 404 Hz with an amplitude of 0.52 mT, controlled by the LIA which drives the power supply to the Helmholtz coils. The whole experiment is controlled using custom-written LabVIEW software.

The use of field modulation and the LIA improves significantly the SNR of the MFE measurements by specifically recording the absorbance oscillating only at the field modulation frequency, thereby discriminating against low frequency noise. However, use of modulation methods precludes the determination of absolute absorbance values (and thus radical concentrations) during the modulated CEAS experiments. All absolute absorbance measurements are made using CRDS, as described above, at  $B=0$ , immediately before modulated CEAS. Unless otherwise stated, the MFE curves shown below were collected in a sequence of 20 repeat scans to improve the SNR.

#### 2.4. Transient absorbance measurements

One of the key purposes of the studies described here is to compare the performance of the modulated CEAS experiment with more conventional experiments for detecting magnetic field effects. Therefore, transient absorbance (TA) measurements were performed on the same DABCO, SDS and thionine system. The laser flash photolysis system has been described previously [38]. In brief, the sample is flowed through a 1 cm

square section Helma quartz flow cell and photo-excited with 532 nm laser pulses from a Continuum Surelite I laser. The monitoring beam from a 300 W Xenon lamp is focused through the sample cell at right angles to the laser excitation and the radical absorbance measured at 405 nm using a monochromator (Oriol) and a Hamamatsu R928 PMT. An in-house C++ software program (Borland C++ Builder) controls a home-built magnetic field controller, optical shutters, and a digital oscilloscope (LeCroy), and records the TA signals at each magnetic field in random order. A home-made macro program is used to calculate the field effects,  $MFE$ , according to:

$$MFE = \frac{1}{t_2 - t_1} \int_{t_1}^{t_2} (A(B, t) - A(0, t)) dt \quad (3)$$

i.e. the difference in TA signals in the presence and absence of an applied magnetic field,  $B$ , integrated over a time interval  $\Delta t = (t_2 - t_1)$ .

### 3. Results and discussion

#### 3.1. Modulated CEAS experiments

Figure 4 shows the  $\text{TH}^*$  absorbance at zero field measured by CRDS as a function of photoexcitation laser power. The right hand axis shows the corresponding thionine radical concentration,  $[\text{TH}^*]_{B=0}$ . The absorbance signal shows signs of reaching a plateau at the higher laser powers corresponding to the saturation onset of the thionine absorption.

Figure 5(a) shows modulated CEAS MFE spectra measured with different 532 nm photoexcitation laser powers for a DABCO, SDS and 20  $\mu\text{M}$  thionine solution. As the data are obtained using phase-sensitive

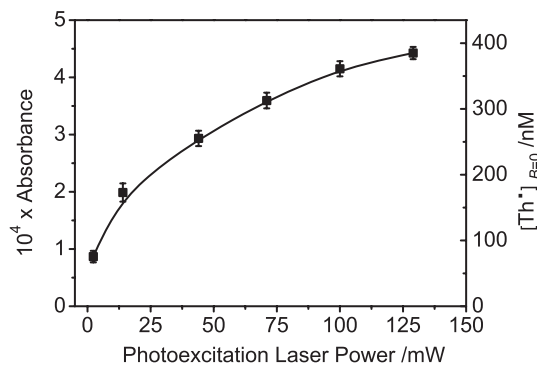


Figure 4. CRDS-measured absorbance of a solution of 2.5  $\mu\text{M}$  thionine in DABCO, SDS, at 405 nm as a function of photoexcitation laser power showing the onset of optical saturation.

detection, the graphs depict the first derivative of the actual magnetic field effects as shown in Figure 1. As expected from Figure 4, at higher photoexcitation laser powers, more  $\text{TH}^*$  is generated resulting in larger observable signals and improved SNR. The spectra are symmetrical with respect to the total magnetic field, the slight offset observed in the figure arises from the presence of the Earth's magnetic field ( $\sim 0.05$  mT). The spectra exhibit high SNR illustrating the benefits of using modulated CEAS in these studies. Both the 'normal' MFE and the LFE (both discussed in more detail below) are clearly observed for 532 nm powers of 14 mW and higher, and as expected the graphs are (apart from a normalisation factor) superimposable as the magnetic properties of the system are laser power independent.

While Figure 4 shows the dependence of  $[\text{TH}^*]_{B=0}$  on the photoexcitation laser power, Figure 5(b) shows

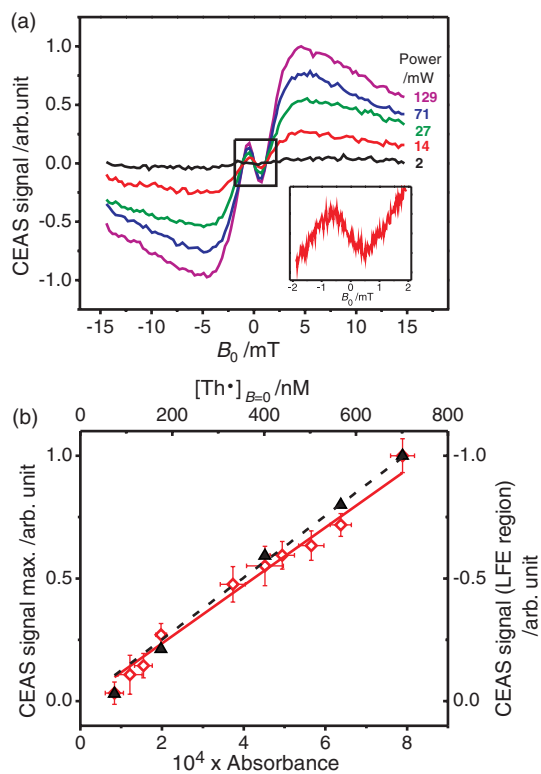


Figure 5. [colour online] (a) CEAS-MFE spectrum of a solution of  $20 \mu\text{M}$  thionine in DABCO, SDS for various 532 nm photoexcitation laser powers. The rectangle in the middle of the figure encloses the low field effect (LFE) and the inset shows the LFE at 14 mW. (b) The CEAS MFE signal maximum at 4.8 mT ( $\diamond$ , left hand scale) and the integrated LFE signal (black triangles, right hand scale), as a function of  $[\text{TH}^*]_{B=0}$ , determined by CRDS. The linear fits are forced through the origin and uncertainties represent one standard deviation (1 s average).

how the modulated CEAS signal varies with  $[\text{TH}^*]_{B=0}$  (top axis) and  $\text{TH}^*$  absorbance (bottom axis). Besides demonstrating the linearity of the modulated CEAS signal with  $[\text{TH}^*]$ , both at the maximum (at 4.8 mT) in the MFE spectrum and integrated over the LFE region, Figure 5(b) permits an estimation of the minimum detectable absorbance (see below).

The improvement in SNR afforded by the use of a high finesse cavity is illustrated in Figure 6, which compares the modulated CEAS signal with that for a single-pass measurement. While no MFE is detected using the single-pass experiment, the modulated CEAS data shows both MFE and LFE with sufficiently high SNR that spectral features are easily quantifiable. In turn this facilitates the extraction of kinetic and spin relaxation information for the spin system studied (see below).

It is an interesting feature of CEAS that, as the losses within the sample represent a significant fraction of the overall loss per round trip, a reduction in the concentration of the sample solution can actually increase the number of passes within the cavity, and hence the sensitivity. The CEF increases as a result of the higher overall finesse of the cavity due to lower scattering and precursor absorption. In these experiments up to 460 passes per ring-down time are achieved with 500 nm thionine solution flowing through the cell. An increase in SNR is best achieved by decreasing the thionine concentration and increasing the photoexcitation power to compensate (within the

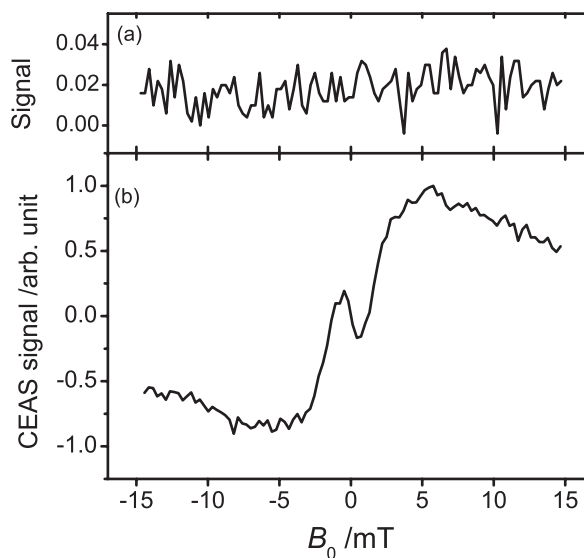


Figure 6. Comparison of (a) modulated single-pass and (b) modulated CEAS-MFE spectra using the same sample solution (DABCO, SDS and  $1 \mu\text{M}$  thionine), photoexcitation power (100 mW) and averaging (50 scan average).



saturation constraints shown in Figure 4). The use of high 532 nm photoexcitation powers (100 mW) in the experimental configuration used here, converts a significant fraction of the thionine within the sample volume to the radical form (*ca.* 20%).

### 3.2. Comparison of modulated CEAS with conventional transient absorption

A major objective of this project was to test the dynamic range of CEAS, with the aim of developing a technique whose superior sensitivity would allow the characterisation of MFEs on smaller and less concentrated samples than are possible using the TA techniques employed previously in the study of such effects. Clearly, though, the proof-of-principle studies must yield the same MFE result as TA under similar conditions. Such comparisons are non-trivial but Figure 7(a) depicts the MFE spectra obtained using both modulated CEAS and single-pass TA for relatively high sample concentrations of thionine (20  $\mu\text{M}$  for the CEAS, 50  $\mu\text{M}$  for the TA) typical of those used in TA measurements. The gratifyingly close agreement between the two sets of data indicates that both methods sample the same radical species. The high SNR in both graphs allows for a straightforward interpretation of all features. Typically, MFEs are characterised by the  $B_{1/2}$  value (defined as the field at half the MFE saturation, see Figure 1) which is often predicted using the Weller formula [41]:

$$B_{1/2} = \sqrt{3} \frac{\langle a_A^2 \rangle + \langle a_B^2 \rangle}{\langle a_A \rangle + \langle a_B \rangle}, \quad (4)$$

with

$$\langle a_X \rangle = \sqrt{\frac{4}{3} \sum_i a_{iX}^2 (I_{iX} + 1) I_{iX}}, \quad (5)$$

where the sum in (5) runs over all  $i$  hyperfine couplings of the radical  $X$  to define  $a_X$ , the effective hyperfine couplings of radical  $X$ . Weller's formula is a 'rule-of-thumb', holding to within a factor of 2 provided the radicals live for neither too long nor too short a time compared with the ST mixing processes [35]. It fails badly, however, if the radicals are subject to fast spin relaxation in which case substantial broadening of the MFE graph is observed. For the hyperfine couplings of thionine [42] and DABCO [43] the estimated  $B_{1/2}$  value of approximately 7 mT does not agree with the experimental results which suggest a much larger  $B_{1/2}$  value: The MFE does not appear to be saturating even at 15.5 mT. Such behaviour is often observed for

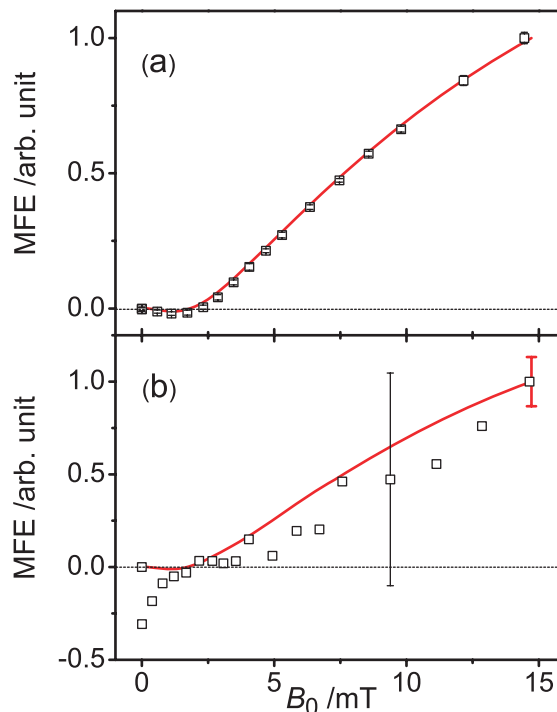


Figure 7. [colour online] (a) Comparison of the modulated CEAS and TA MFE spectra for comparatively high concentrations of thionine in DABCO, SDS showing close agreement of the two techniques. The solid line is the 20 scan average of the modulated CEAS data with  $[\text{TH}^+]_{B=0} = 690 \pm 14 \text{ nM}$ . The TA data ( $\square$ ) were obtained by integrating the flash photolysis data using a boxcar window with  $\Delta t = 6 \mu\text{s}$  centred at  $5 \mu\text{s}$  after the 20 mJ laser flash and represent 1000 shot averages per point. (b) Comparison of modulated CEAS and TA MFE spectra for the same solution of  $1 \mu\text{M}$  thionine in DABCO, SDS. The solid line is the modulated CEAS data, collected with  $[\text{TH}^+]_{B=0} = 157 \pm 12 \text{ nM}$ , average of 50 scans. The TA data ( $\square$ ) were obtained as in (a) but with 170 shot average per point for more direct comparison with the CEAS data (see text). The TA spectrum shown is the averaged result of 20 such traces the standard deviation of which is displayed for one data point as a representative uncertainty.

radical species confined to micelles and is typically explained by a contribution of two different mechanisms – the hyperfine mechanism [9,44] and the relaxation mechanism [9,44,45] leading to a broadening of the MFE spectrum far beyond that predicted by the Weller formula. Further information as to the role played by both mechanisms may be extracted through sophisticated analysis of MFE data obtained by time-resolved and pulsed techniques [46] but is beyond the scope of this work.

Figure 7(b) provides a comparison of the two techniques at low precursor concentrations ( $1 \mu\text{M}$   $\text{TH}^+$ ). To allow as reliable a comparison between TA and CEAS as possible, the data are

obtained under as close to identical recording conditions as possible; *via* the number of repeat scans averaged it is ensured that the total integrated photoexcitation energy used during the course of the TA experiment (1360 J) is comparable to that used in modulated CEAS (1380 J). As a result, solutions in the two experiments are subject to similar numbers of photons and the results thus provide a reasonable comparison of the relative sensitivities of the two methods. The standard deviation in the integrated CEAS data is displayed on the right hand edge of the curve. Judging from the SNR in Figure 7(b), the quality of the data from the modulated CEAS experiment is demonstrably superior to that achieved using the traditionally employed single pass TA apparatus.

As this is the first application of cavity-based techniques to the study of magnetic field effects it is worth considering the improvements they provide and the sensitivity which might ultimately be achieved. The minimum detectable absorbance per pass achieved using CRDS with pure water in the cell, may be determined from

$$A_{\min} = \frac{\Delta\tau_{\min}L}{2.3026c\tau_0^2}, \quad (6)$$

where  $\Delta\tau_{\min}$  is the minimum detectable change in the ring down time. Determining  $\Delta\tau_{\min}$  from three standard deviations in the baseline noise over a 1 s time, yields a minimum detectable absorbance per pass of  $3.2 \times 10^{-8}$ , which is in line with previous liquid cell CRDS measurements (see Table II in [32]). However, the same measurements made when flowing a solution of 500 nM thionine in DABCO, SDS solution yield a value of only  $2 \times 10^{-5}$ . There are multiple reasons for this marked decrease in sensitivity: The sample solution introduces scattering, which, as well as producing instability in the measurements (i.e. noise, which increases markedly the smallest detectable change in the ring-down time), reduces the base ring-down time,  $\tau_0$ , by approximately a factor of two as discussed in Section 2.3. It follows from expression (6) that this significantly affects  $A_{\min}$ . For comparison, the minimum detectable absorbance change in the TA experiment is estimated to be  $1.5 \times 10^{-4}$ , i.e. comparable with the CRDS measurements.

By virtue of the use of modulation techniques employed, it is less easy to be quantitative regarding the limits of detection using the modulated CEAS. Ultimately, the improvement modulated CEAS provides over TA is illustrated by the improved SNR in Figure 7(b) and the fact that an MFE could be observed using modulated CEAS in more dilute solutions than were amenable to TA measurements.

Using modulated CEAS, it was possible to clearly observe the MFE (including LFE component) for a solution of 500 nM thionine (generating  $[\text{TH}^*]_{B=0} = 98 \text{ nM}$ , detectable by CRDS) which was comfortably beyond the detection limits of our TA measurements.

By comparing data recorded for similar solutions, it is possible to estimate the relative sensitivities of CRDS, CEAS and modulated CEAS as implemented here. For a comparison of CRDS and un-modulated CEAS we have measured the  $\text{TH}^*$  absorbance at zero field for a solution of  $1 \times 10^{-6} \text{ M}$  thionine (generating  $[\text{TH}^*]_{B=0} = 306 \text{ nM}$ ). In this comparison the CEAS proves the more sensitive by a factor of 5.3. This is initially surprising as CRDS is usually considered the (slightly) more sensitive of the two techniques. However, at the light levels and ring-down time used here, detector noise and uncertainties in fitting fast exponential decays are significant limiting factors in the CRDS measurements. Indeed, for the substantial per pass losses encountered in these studies for working solutions, the dynamic range of the CEAS technique is better than that of CRDS for the reasons discussed above.

The change in radical absorbance upon application of a  $B_0 = 10 \text{ mT}$  field to the same solution was also measured by all three cavity-based techniques. In this case, CRDS is unable to discern the additional signal due to the applied field but the effect of introducing the field modulation to the CEAS measurements is to increase the SNR by an additional factor of *ca* 5.

While modulated CEAS benefits from the gains in signal to noise described above due to both its CW nature and the well-known advantages of phase-sensitive detection, TA retains the advantage that its measurements are exclusively sensitive to  $\text{TH}^*$  decay and insensitive to scattering losses. By comparison, modulated CEAS probes the steady state  $\text{TH}^*$  absorbance change that results from both  $\text{TH}^*$  decay and the (magnetic field insensitive)  $\text{TH}^*$  generation process.

#### 4. Conclusions and outlook

The main objective of this work was to test the applicability of cavity-based optical techniques for the study of magnetic field effects in solution. In the application described here, CEAS results in a clear improvement in terms of sensitivity compared with conventional TA based methods.

The apparatus used here is a first prototype only, constructed from components available within the groups involved for the purpose of these proof-of-principle studies. Most experimental parameters

are yet to be optimised. The number of passes of light within the cavity and, therefore, the enhancement in sensitivity, is limited primarily by the presence of the intra-cavity sample cell, the optical quality of whose surfaces are far inferior to those usually used in CEAS and CRDS studies. Additional losses arise from scattering and absorption in the micelles themselves. It is likely that major gains in sensitivity could be achieved with the use of homogeneous solution and anti-reflection coated, custom-made optical cells [28]. Alternatively, coating the cell walls as the highly reflective mirrors would create a microcavity with fewer intracavity elements, thereby increasing the finesse and, ultimately, the sensitivity.

It should, however, also be recognised that the thionine system was carefully chosen for these initial experiments. It has two advantageous aspects for this purpose: Firstly, the system exhibits long radical lifetimes and, therefore, comparatively large nascent radical concentrations. Transient absorbance measurements also permit the study of short-lived species to which the CEAS techniques, as implemented here, would be less ideally suited. Secondly, in direct absorption experiments, it is a major advantage that the ground state of thionine has negligible absorption at the detection wavelength. Overlap of absorption bands of radical and precursor species, is, however, quite common. As modulated CEAS is currently limited to regions in which a suitable light source is available, the number of systems which might benefit from the sensitivity gains demonstrated may be somewhat restricted. However, ultra broadband variants of CEAS utilising supercontinuum sources are currently being developed within this group for use in condensed phases [47,48]. In addition, incoherent light sources (lamps, LEDs, etc.) can also be used, thus reducing the cost and complexity of a typical instrument [32,49–51]. Thus, with the application of broadband cavity mirrors and multiple excitation wavelengths, the number of systems benefiting from the application of CEAS will increase dramatically.

One promising aspect of the sensitivity gains CEAS offers is in the possibilities it affords for miniaturisation. Proteins such as cryptochromes and photolyases can often only be produced in nano to (few) micromolar concentrations which, according to this study, may be accessible to CEAS techniques. This eliminates the need for bulk production as required by TA methodology. The MFE experiments on the TA apparatus require millilitre volumes of solutions containing around 100 micromolar (or more) of photoactive compound, a demand often beyond the reasonable capability of synthetic labs. Cavity-based

techniques, therefore, offer new possibilities in the investigation of biological samples in this field.

In the present modulated CEAS cavity, the sample volume probed is estimated to be *ca* 5  $\mu\text{L}$ . It is easy to conceive of an evanescent-wave (EW) cavity-based technique such as those employing intra-cavity prisms [3,26,52–56] which could be applied allowing sample volumes in the nanolitre range to be probed. EW cavity-based techniques offer the possibility of polarisation sensitive absorption, which might be a promising direction for the future study of magnetic field effects in oriented thin films mimicking biological systems hypothesised to function as biological magnetic compasses.

### Acknowledgements

We are grateful for the financial support this work has received from the Engineering and Physical Sciences Research Council (EPSRC), the Royal Society and the EMF Biological Research Trust. SRM is further grateful to the EPSRC for his Advanced Research Fellowship. We are indebted to Professor Ulrich Steiner for helpful discussions.

### References

- [1] A.J. Hoff, *Q. Rev. Biophys.* **14**, 599 (1981).
- [2] R. Haberkorn and M.E. Michelbeyerle, *Biophys. J.* **26**, 489 (1979).
- [3] Y. Liu, R. Edge, K. Henbest, C.R. Timmel, P.J. Hore and P. Gast, *Chem. Commun.* **2**, 174 (2005).
- [4] J.R. Woodward, T.J. Foster, A.R. Jones, A.T. Salaoru and N.S. Scrutton, *Biochem. Soc. Trans.* **37**, 358 (2009).
- [5] C.T. Lin and D. Shalitin, *Annu. Rev. Plant Biol.* **54**, 469 (2003).
- [6] C.T. Lin and T. Todo, *Genome Biol.* **6**, 9 (2005).
- [7] T. Ritz, S. Adem and K. Schulten, *Biophys. J.* **78**, 707 (2000).
- [8] K.B. Henbest, K. Maeda, P.J. Hore, M. Joshi, A. Bacher, R. Bittl, S. Weber, C.R. Timmel and E. Schleicher, *Proc. Nat. Acad. Sci. USA* **105**, 14395 (2008).
- [9] U.E. Steiner and T. Ulrich, *Chem. Rev.* **89**, 51 (1989).
- [10] C.R. Timmel and K.B. Henbest, *Philos. Trans. R. Soc. London, Series a-Math. Phys. Eng. Sci.* **362**, 2573 (2004).
- [11] J.R. Woodward, C.R. Timmel, K.A. McLaughlan and P.J. Hore, *Phys. Rev. Lett.* **87**, 077602 (2001).
- [12] J.R. Woodward, *Prog. Reaction Kinetics Mech.* **27**, 165 (2002).
- [13] A. Okeefe and D.A.G. Deacon, *Rev. Sci. Instrum.* **59**, 2544 (1988).
- [14] G. Berden, R. Peeters and G. Meijer, *Int. Rev. Phys. Chem.* **19**, 565 (2000).

- [15] M.D. Wheeler, S.M. Newman, A.J. Orr-Ewing and M.N.R. Ashfold, *J. Chem. Soc. – Faraday Trans.* **94**, 337 (1998).
- [16] R. Engeln, G. Berden, R. Peeters and G. Meijer, *Rev. Sci. Instrum.* **69**, 3763 (1998).
- [17] A. O’Keefe, *Chem. Phys. Lett.* **293**, 331 (1998).
- [18] C. Vallance, *New J. Chem.* **29**, 867 (2005).
- [19] L. van der Sneppen, F. Ariese, C. Gooijer and W. Ubachs, *Annu. Rev. Anal. Chem.* **2**, 13 (2009).
- [20] S. Xu, G. Sha and J. Xie, *Rev. Sci. Instrum.* **73**, 255 (2002).
- [21] A.J. Hallock, E.S.F. Berman and R.N. Zare, *Anal. Chem.* **74**, 1741 (2002).
- [22] A.J. Hallock, E.S.F. Berman and R.N. Zare, *J. Am. Chem. Soc.* **125**, 1158 (2003).
- [23] A.J. Alexander, *Anal. Chem.* **78**, 5597 (2006).
- [24] A.M. Shaw, T.E. Hannon, F. Li and R.N. Zare, *J. Phys. Chem. B* **107**, 7070 (2003).
- [25] A.C.R. Pipino, J.W. Hudgens and R.E. Huie, *Rev. Sci. Instrum.* **68**, 2978 (1997).
- [26] M. Mazurenka, L. Wilkins, J.V. Macpherson, P.R. Unwin and S.R. Mackenzie, *Anal. Chem.* **78**, 6833 (2006).
- [27] A.J. Alexander, *Chem. Phys. Lett.* **393**, 138 (2004).
- [28] K.L. Snyder and R.N. Zare, *Anal. Chem.* **75**, 3086 (2003).
- [29] K.L. Bechtel, R.N. Zare, A.A. Kachanov, S.S. Sanders and B.A. Paldus, *Anal. Chem.* **77**, 1177 (2005).
- [30] L. van der Sneppen, F. Ariese, C. Gooijer and W. Ubachs, *J. Chromatog. A* **1148**, 184 (2007).
- [31] S.E. Fiedler, A. Hese and A.A. Ruth, *Chem. Phys. Lett.* **371**, 284 (2003).
- [32] M. Islam, L.N. Seetohul and Z. Ali, *Appl. Spectrosc.* **61**, 649 (2007).
- [33] B. Brocklehurst, *J. Chem. Soc. -Faraday Trans.* **72**, 1869 (1976).
- [34] C.R. Timmel, U. Till, B. Brocklehurst, K.A. McLauchlan and P.J. Hore, *Mol. Phys.* **95**, 71 (1998).
- [35] C.T. Rodgers, S.A. Norman, K.B. Henbest, C.R. Timmel and P.J. Hore, *J. Am. Chem. Soc.* **129**, 6746 (2007).
- [36] K.A. McLauchlan and U.E. Steiner, *Mol. Phys.* **73**, 241 (1991).
- [37] B. van Dijk, J.K.H. Carpenter, A.J. Hoff and P.J. Hore, *J. Phys. Chem. B* **102**, 464 (1998).
- [38] K. Maeda, K.B. Henbest, F. Cintolesi, I. Kuprov, C.T. Rodgers, P.A. Liddell, D. Gust, C.R. Timmel and P.J. Hore, *Nature* **453**, 387 (2008).
- [39] U. Steiner, G. Winter and H.E.A. Kramer, *J. Phys. Chem.* **81**, 1104 (1977).
- [40] M. Goetz, K.B. Henbest, E.G. Windham, K. Maeda and C.R. Timmel, *Chem. Eur. J.* **15**, 6058 (2009).
- [41] A. Weller, F. Nolting and H. Staerk, *Chem. Phys. Lett.* **96**, 24 (1983).
- [42] L.D. Tuck and D.W. Schieser, *J. Phys. Chem.* **66**, 937 (1962).
- [43] M. Kaise and K. Someno, *Chem. Lett.* **7**, 1295 (1987).
- [44] Y.N.M.K.M. Salikov, R.Z. Sagdeev and A.L. Buchachenko, editors, *Spin Polarisation and Magnetic Effect in Radical Reactions* (Elsevier, Amsterdam, 1984).
- [45] H. Hayashi and S. Nagakura, *Bull. Chem. Soc. Jpn* **57**, 322 (1984).
- [46] K. Maeda, T. Miura and T. Arai, *Mol. Phys.* **104**, 1779 (2006).
- [47] M. Schnippering, P.R. Unwin, J. Hult, T. Laurila, C.F. Kaminski, J.M. Langridge, R.L. Jones, M. Mazurenka and S.R. Mackenzie, *Electrochem. Commun.* **10**, 1827 (2008).
- [48] L. van der Sneppen, G. Hancock, C. Kaminski, T. Laurila, S.R. Mackenzie, S.R.T. Neil, R. Peverall, G.A.D. Ritchie, M. Schnippering and P.R. Unwin, *Analyst* **135**, 133 (2010).
- [49] L.N. Seetohul, Z. Ali and M. Islam, *Anal. Chem.* **81**, 4106 (2009).
- [50] S.E. Fiedler, A. Hese and A.A. Ruth, *Rev. Sci. Instrum.* **76**, 089901 (2005).
- [51] A.A. Ruth and K.T. Lynch, *Phys. Chem. Chem. Phys.* **10**, 7098 (2008).
- [52] A.C.R. Pipino, J.W. Hudgens and R.E. Huie, *Chem. Phys. Lett.* **280**, 104 (1997).
- [53] T.E. Hannon, S. Chah and R.N. Zare, *J. Phys. Chem. B* **109**, 7435 (2005).
- [54] H.V. Powell, M. Schnippering, M. Mazurenka, J.V. Macpherson, S.R. Mackenzie and P.R. Unwin, *Langmuir* **25**, 248 (2009).
- [55] M. Schnippering, H.V. Powell, M. Zhang, J.V. Macpherson, P.R. Unwin, M. Mazurenka and S.R. Mackenzie, *J. Phys. Chem. C* **112**, 15274 (2008).
- [56] M. Mazurenka, S.M. Hamilton, P.R. Unwin and S.R. Mackenzie, *J. Phys. Chem. C* **112**, 6462 (2008).